Experimental Hematology

Experimental Hematology 2019;73:1–6

BRIEF COMMUNICATION

Eltrombopag promotes DNA repair in human hematopoietic stem and progenitor cells

Kacey L. Guenther[a], Patali S. Cheruku[a], Ayla Cash[a], Richard H. Smith[a], Luigi J. Alvarado[a], Sandra Burkett[b], Danielle M. Townsley[a], Thomas Winkler[a], and Andre Larochelle[a]

[a]*National Heart, Lung and Blood Institute, National Institutes of Health, Bethesda, MD;* [b]*National Cancer Institute, National Institutes of Health, Frederick, MD*

(Received 4 February 2019; revised 14 March 2019; accepted 16 March 2019)

A causal link between hematopoietic stem/progenitor cell (HSPC) dysfunction and DNA damage accrual has been proposed. Clinically relevant strategies to maintain genome integrity in these cells are needed. Here we report that eltrombopag, a small molecule agonist of the thrombopoietin (TPO) receptor used in the clinic, promotes DNA double-strand break (DSB) repair in human HSPCs. We found that eltrombopag specifically activates the classic nonhomologous end-joining (C-NHEJ) DNA repair mechanism, a pathway known to support genome integrity. Eltrombopag-mediated DNA repair results in enhanced genome stability, survival, and function of primary human HSPCs, as demonstrated in karyotyping analyses, colony-forming unit assays and after transplantation in immunodeficient NSG mice. Eltrombopag may offer a new therapeutic modality to protect human HSPCs against genome insults. Published by Elsevier Inc. on behalf of ISEH – Society for Hematology and Stem Cells.

Maintenance of genome integrity is crucial to preserve the function of long-term repopulating hematopoietic stem and progenitor cells (HSPCs) for lifelong blood production. DNA double-strand breaks (DSBs) are well-studied cytotoxic DNA alterations that may arise from exposure to cancer therapies, such as ionizing radiation (IR) and chemotherapeutic agents, or from endogenous products of metabolic activities, such as reactive oxygen species (ROS).

There are two primary mechanisms underlying repair of DNA DSBs: homologous recombination (HR) and nonhomologous end joining (NHEJ) [1,2]. In HSPCs, NHEJ is the prominent repair mechanism [3–5]. This pathway is generally considered error-prone, in contrast to the error-free HR mechanism. However, this view has been challenged by the recent description of an alternative NHEJ (alt-NHEJ) mechanism, distinct from the classic or canonical NHEJ (C-NHEJ) pathway [6]. The classic form of NHEJ is a fast-operating process. The DNA-dependent protein kinase (DNA-PK) and ligase IV/XRCC4/XLF complexes are principal enzymatic components of this pathway [7,8]. In contrast, alt-NHEJ repairs DNA DSBs with much slower kinetics, and the enzymatic requirements are distinct from those implicated in C-NHEJ. The alt-NHEJ mechanism is considered to be a backup pathway, gaining functional relevance in DNA DSB repair when C-NHEJ fails [9–12]. This alternative pathway is highly mutagenic [13–15], accounting for the reported fallibility of NHEJ [16–18]. In contrast, C-NHEJ is associated with more limited and infrequent

KLG and PSC contributed equally. KLG, PSC, AC, and AL conceived and designed the study. KLG, PSC, AC, RHS, LJA, SB, and AL performed the experimental procedures and analyzed the data. DMT and TW provided helpful suggestions. KLG, PSC, and AL wrote and edited the article with contributions from all other authors.

Offprint requests to: Andre Larochelle, MD, PhD, National Heart, Lung and Blood Institute, National Institutes of Health, Bethesda, 9000 Rockville, Bethesda, MD 20892; E-mail: larochea@nhlbi.nih.gov

Supplementary material associated with this article can be found, in the online version, at https://doi.org/10.1016/j.exphem.2019.03.002.

0301-472X/Published by Elsevier Inc. on behalf of ISEH – Society for Hematology and Stem Cells.
https://doi.org/10.1016/j.exphem.2019.03.002

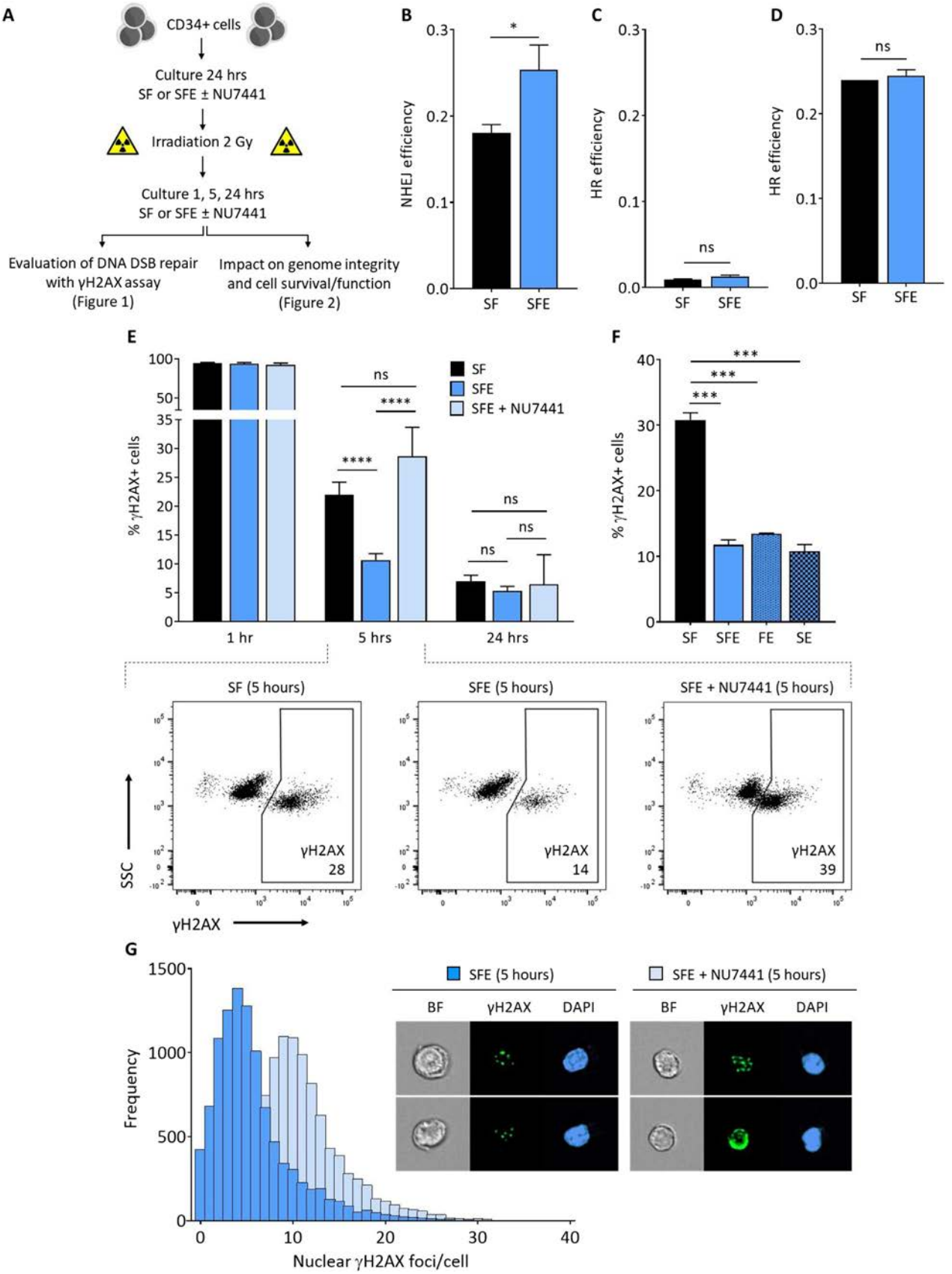
A
CD34+ cells
Culture 24 hrs
SF or SFE ± NU7441
Irradiation 2 Gy
Culture 1, 5, 24 hrs
SF or SFE ± NU7441
Evaluation of DNA DSB repair with γH2AX assay (Figure 1)
Impact on genome integrity and cell survival/function (Figure 2)
B
NHEJ efficiency
SF
SFE
C
HR efficiency
ns
D
HR efficiency
ns
E
% γH2AX+ cells
SF
SFE
SFE + NU7441
1 hr
5 hrs
24 hrs
F
% γH2AX+ cells
SF
SFE
FE
SE
SF (5 hours)
SFE (5 hours)
SFE + NU7441 (5 hours)
SSC
γH2AX
γH2AX 28
γH2AX 14
γH2AX 39
G
Frequency
Nuclear γH2AX foci/cell
SFE (5 hours)
SFE + NU7441 (5 hours)
BF
γH2AX
DAPI

alterations in sequence at the repair junctions and is considered to be critical in maintaining genome stability [16,18,19].

Recent investigations have uncovered a specific function of thrombopoietin (TPO), a primary regulator of HSPC survival, in promoting C-NHEJ–mediated DNA DSB repair in these cells [20,21]. Short exposure of murine HSPCs to TPO prior to low-dose IR protected cells against genome instability and partially rescued their loss of function. These data implied that activating the TPO signaling axis in HSPCs prior to therapy with anticancer agents may offer clinical benefits by reducing the risks of HSPC injury and secondary hematological malignancies. Recombinant TPO is not available for clinical use, but the synthetic small molecule mimetic of TPO, eltrombopag, was recently reported to stimulate multipotent long-term repopulating HSPCs in patients with bone marrow (BM) failure [22,23], resulting in persistent trilineage hematopoiesis. In this study, we investigated whether eltrombopag also promotes DNA repair in human HSPCs.

Methods

An overview of study design is found in Figure 1A, and methods are detailed in the Supplementary Material (online only, available at www.exphem.org).

Evaluation of DNA DSB repair

CD34+ cells were obtained from healthy individuals after informed consent under an institutional review board–approved clinical protocol. Cells were cultured for 24 hours in the presence of cytokines, stem cell factor (SCF), and Flt3L (SF) or SF supplemented with eltrombopag (SFE) with or without DNA-PK inhibitor (NU7441), prior to induction of DNA DSBs by exposure to low-dose (2 Gy) IR. To assess the kinetics of DNA repair, cultures were continued for an additional 1, 5, and 24 hours after IR, and cells were stained with anti-phospho-histone (H2A.X) prior to data collection by flow cytometry. To distinguish between NHEJ and HR, CD34+ cells were electroporated with either NHEJ-GFP or HR-GFP reporter plasmids [24] and tdTomato plasmids as internal control. Efficiency of DNA repair was expressed as the ratio of GFP + tdTomato+ cells to total tdTomato+ cells. For multispectral imaging flow cytometry, cells were incubated overnight with H2A.X and stained with DAPI prior to capture on ImageStream.

Evaluation of cellular genome integrity, survival, and function

To assess genome integrity, chromosomal aberrations were blindly examined in CD34+ cell metaphase spreads. To quantify cellular survival, cells were stained with Annexin V/viability dye. Gene expression analysis was performed using a custom Qiagen RT^2 Profiler PCR Array in CD34+ cells collected 5 hours after IR. To measure progenitor function, CD34+ cells were plated in MethoCult Medium and colonies were scored after 10–14 days. To assess long-term repopulating potential, HSPCs were injected intravenously into sublethally irradiated NSG mice on a study protocol approved by the Animal Care and Use Committee (ACUC) of the National Heart, Lung and Blood Institute (NHLBI). Bone marrow cells were stained with anti-CD45-PE to quantify human cell engraftment 12 weeks post-transplantation.

Results and discussion

To assess whether eltrombopag promotes DNA DSB repair in human HSPCs and to identify the pathways involved, CD34+ cells obtained from healthy individuals were first cultured for 24 hours in the presence or absence of eltrombopag, exposed to low dose (2 Gy) IR, and transfected with NHEJ or HR DNA DSB repair reporter plasmids [24]. Eltrombopag significantly improved NHEJ activity after IR (Figure 1B; Supplementary Figure E1, online only, available at www.exphem.org). Because DNA DSBs are repaired by HR only in the late S/G2 phase of the cell cycle, we examined the efficiency of HR in actively dividing CD34+ cells (Figure 1C) and c-MPL–expressing HEL 92.1.7 cells (Figure 1D). Eltrombopag did not promote HR activity after IR in these cells.

Figure 1. Eltrombopag promotes the C-NHEJ DNA DSB repair mechanism in human HSPCs. **(A)** Experimental procedure. Human CD34+ cells were collected by apheresis of normal volunteers after G-CSF mobilization. The γH2AX assay was used to evaluate DNA DSB repair 1, 5, and 24 hours after 2-Gy IR, following a 24-hour culture in the presence of early-acting cytokines (SCF and Flt3L, designated SF) or SF supplemented with eltrombopag (SFE) with and without DNA-PK inhibitor (NU7441). Mock-irradiated cells were processed and cultured following the same procedure, but not exposed to IR. Results of DNA DSB repair activity and underlying mechanisms are presented in *Figure 1,* and data illustrating the impact of DSB repair on genome integrity, cell survival, and function are shown in *Figure 2*. **(B)** Efficiency of NHEJ DNA repair in human HSPCs cultured with SF or SFE for 24 hours before IR and electroporation of reporter plasmids ($n = 3$). **(C)** Efficiency of HR DNA repair in human HSPCs cultured for 96 hours to enhance cell cycling before IR and electroporation of reporter plasmids ($n = 3$). **(D)** Efficiency of HR DNA repair in actively cycling c-MPL–expressing HEL 92.1.7 cells cultured for 96 hours before IR and electroporation of reporter plasmids ($n = 3$). **(E)** Summary of H2AX phosphorylation (γH2AX) 1, 5, and 24 hours after 2-Gy IR of human HSPCs cultured with SF, SFE, or SFE + NU7441 ($n = 24$, from 13 independent donors). *Insets:* Representative γH2AX immunostaining flow cytometry plots indicating that addition of the DNA-PK inhibitor NU7441 during culture completely abrogated the enhanced kinetics of DNA DSB repair observed at 5 hours with eltrombopag in HSPCs compared with the SF control group (*bottom*). The flow cytometry gating strategy is provided in *Supplementary Figure E3A* (online only, available at www.exphem.org). **(F)** Summary percentages of γH2AX+ cells at 5 hours post-IR of human HSPCs cultured in SF, SFE, FE (Flt3L and eltrombopag but no SCF), or SE (SCF and eltrombopag but no Flt3L) ($n = 3$). **(G)** Frequencies of nuclear γH2AX foci detected per cell at 5 hours post-IR using multispectral imaging flow cytometry in human HSPCs cultured with SFE in the presence or absence of NU7441. An image representative of three experiments is shown. *Insets:* Bright-field (BF) images, γH2AX foci, and DAPI nuclear staining of representative cells. In **(B)**–**(F)**, results are expressed as the mean ± SEM. $*p < 0.05$, $***p < 0.001$, $****p < 0.0001$ by unpaired Student *t* tests; ns=Not significant.

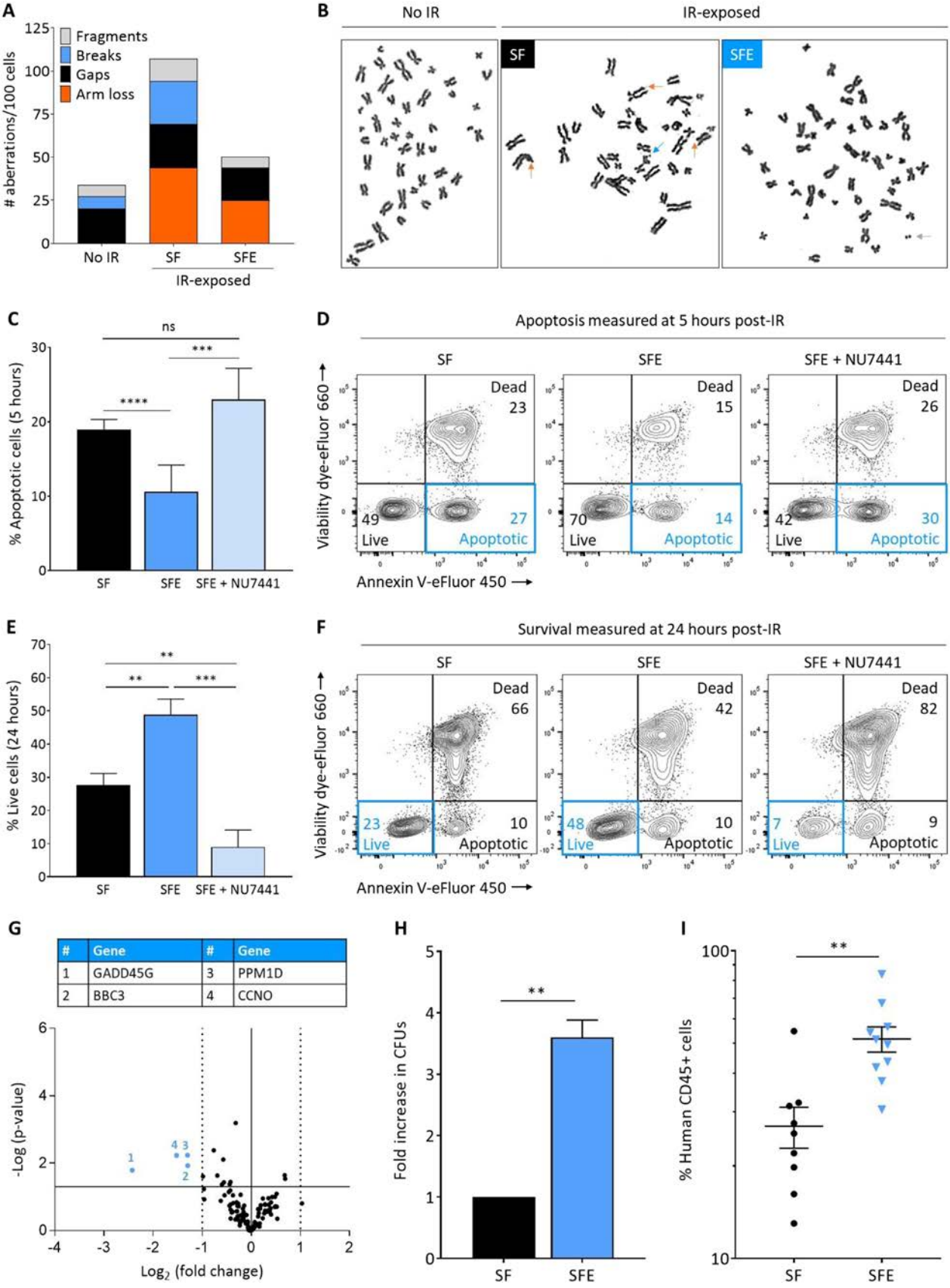
A
aberrations/100 cells
Fragments
Breaks
Gaps
Arm loss
No IR
SF
SFE
IR-exposed
B
No IR
IR-exposed
SF
SFE
C
% Apoptotic cells (5 hours)
ns
***
****
SF
SFE
SFE + NU7441
D
Apoptosis measured at 5 hours post-IR
SF
SFE
SFE + NU7441
Viability dye-eFluor 660
Annexin V-eFluor 450
Dead 23
49 Live
27 Apoptotic
Dead 15
70 Live
14 Apoptotic
Dead 26
42 Live
30 Apoptotic
E
% Live cells (24 hours)
**
***
F
Survival measured at 24 hours post-IR
Dead 66
23 Live
10 Apoptotic
Dead 42
48 Live
10 Apoptotic
Dead 82
7 Live
9 Apoptotic
G
Gene # Gene
1 GADD45G 3 PPM1D
2 BBC3 4 CCNO
-Log (p-value)
Log2 (fold change)
H
Fold increase in CFUs
I
% Human CD45+ cells

To distinguish between the fast-operating C-NHEJ and slower-kinetics alt-NHEJ repair mechanisms, CD34+ cells were cultured and irradiated as previously described and then assessed for changes in H2AX phosphorylation (γH2AX), an indicator of IR-induced DSBs, at various times after IR. Maximal percentages of H2AX phosphorylation were observed 1 hour after IR for both culture conditions, indicating that eltrombopag does not prevent DNA DSB formation in HSPCs (Figure 1E). Five hours after IR, most cells cultured with eltrombopag had resolved DNA DSBs, while twofold higher percentages of γH2AX+ cells persisted in the control group (Figure 1E). The observed effect was specific to eltrombopag; removal of other cytokines did not prevent DNA repair (Figure 1F). By 24 hours post-IR, the control group had similarly resolved DNA DSBs, implying that DNA repair occurred via a slower-acting pathway in the absence of eltrombopag (Figure 1E). Similar results were obtained when cultures were supplemented with TPO (Supplementary Figure E2, online only, available at www.exphem.org).

To confirm that eltrombopag enhances repair of DNA DSBs in irradiated human HSPCs by promoting a pathway with fast kinetics, we inhibited DNA-PK, a kinase specific to the fast-operating C-NHEJ pathway [7]. Addition of the DNA-PK inhibitor NU7441 during culture had no impact on DNA DSB formation measured at 1 hour or on DNA repair at 24 hours, but completely abrogated the enhanced kinetics of DNA DSB repair observed at 5 hours with eltrombopag in HSPCs (Figure 1E). To further corroborate these findings, we examined nuclear γH2AX foci at single-cell resolution using multispectral imaging flow cytometry. The frequencies of γH2AX foci detected per HSPC at 5 hours post-IR in the presence of eltrombopag were also found to be markedly increased when NU7441 was added during culture (Figure 1G). These results establish that eltrombopag enhances the baseline fast-operating DNA-PK–dependent C-NHEJ DNA repair mechanism measured at 5 hours in human HSPCs. In contrast, in the absence of eltrombopag, more cells resolve DNA DSBs using the slower, DNA-PK–independent and error-prone alt-NHEJ mechanism measured at 24 hours.

We next investigated the impact of promoting C-NHEJ repair on genome integrity, cell survival, and function of irradiated HSPCs. Metaphases prepared from irradiated HSPCs cultured with eltrombopag exhibited significantly fewer chromosomal aberrations than irradiated cells cultured in the absence of eltrombopag and only minimally increased aberrations relative to cultured HSPCs not exposed to IR (Figure 2A,B). Addition of eltrombopag during culture was also associated with a substantial decrease in apoptosis (measured at 5 hours, Figure 2C,D) and enhanced survival (measured at 24 hours, Figure 2E,F) of irradiated HSPCs compared with control groups. When C-NHEJ DNA repair was inhibited with NU7441, the cell survival benefit observed with eltrombopag was abolished (Figure 2C–F). To corroborate these findings, we identified 128 genes involved in DNA damage signaling, cell cycle regulation, apoptosis, or DNA repair (Supplementary Table E1, online only, available at www.exphem.org), and compared their expression by reverse transcription quantitative polymerase chain reaction (RT-qPCR) arrays in irradiated HSPCs cultured with or without eltrombopag. Five hours after IR, cells cultured with eltrombopag exhibited a significant (three- to sixfold) decrease in expression of four pro-apoptotic and growth-inhibiting genes, namely, GADD45G, BBC3, PPM1D, and CCNO, compared with HSPCs cultured without eltrombopag (Figure 2G). To evaluate the functional relevance of these findings, cells were assessed in CFU progenitor assays and by transplantation into NSG mice. In CFU assays, irradiated HSPCs cultured with eltrombopag yielded three- to fourfold more CFUs than control groups (Figure 2H). In xenograft assays, a twofold increase in human cell engraftment was observed 3 months after transplantation of IR-exposed HSPCs cultured in the presence of eltrombopag compared with control groups (Figure 2I).

In conclusion, this study builds on the previous demonstration that TPO promotes DNA repair in murine HSPCs and extends this finding to a clinically relevant c-MPL agonist, eltrombopag, in human progenitors and cells with

Figure 2. Eltrombopag-mediated DNA DSB repair results in enhanced genome stability, survival, and function of human HSPCs. **(A)** Quantification of chromosomal aberrations on metaphase spreads of human CD34+ cells cultured as described in *Figure 1A* with SF or SFE prior to 2-Gy IR. No IR control CD34+ cells were subjected to the same culture conditions with SFE, but not exposed to IR. Chromosomal aberrations observed in the no IR group result from the prolonged ex vivo cultures required for karyotyping analyses. **(B)** Representative metaphase spreads of human CD34+ cells showing chromosomal aberrations marked with *arrows*. Color of each arrow refers to a specific aberration, as defined in the legend in *Figure 2A*. **(C)** Summary of percentages of apoptotic cells 5 hours post-IR of human HSPCs cultured with SF, SFE, or SFE + NU7441 ($n = 15$, from 11 independent donors). **(D)** Representative cell viability flow cytometry plots obtained by dual annexin V/viability dye immunostaining at 5 hours post-IR of human HSPCs cultured with SF, SFE, or SFE + NU7441. **(E)** Summary of percentages of live cells 24 hours post-IR of human HSPCs cultured with SF, SFE, or SFE + NU7441 ($n = 15$, from 11 independent donors). **(F)** Representative cell viability flow cytometry plots obtained by dual annexin V/viability dye immunostaining 24 hours post-IR of human HSPCs cultured with SF, SFE, or SFE + NU7441. The flow cytometry gating strategy is shown in *Supplementary Figure E3B* (online only, available at www.exphem.org). **(G)** Volcano plot showing gene expression data at 5 hours post-IR of human HSPCs cultured with SFE compared with SF ($n = 3$). The x- and y-axes show gene expression fold-change of SFE versus SF and statistical significance, respectively. Each point represents an individual gene. The *solid horizontal line* shows where $p = 0.05$; for points above the line, $p < 0.05$, and for points below the line, $p > 0.05$. The *solid vertical line* shows where fold-change = 1 and the *dashed vertical lines* indicate where fold-change is >twofold. The colored numbered points indicate genes of interest that display both >twofold changes in expression and high statistical significance. All results were normalized based on GAPDH expression. **(H)** Fold increase in colony-forming units (CFUs) counted 10–14 days after plating human HSPCs cultured and irradiated as previously described; data were normalized to the SF control group. **(I)** Human cell engraftment as measured by human CD45-expressing cells in the bone marrow of immunodeficient recipient (NSG) mice 12 weeks after transplantation of human HSPCs cultured and irradiated as previously described. Each *dot* represents an individual mouse ($n = 19$ mice). In **(C)**, **(E)**, **(H)**, and **(I)**, results are expressed as the mean ± SEM. $^{**}p < 0.01$, $^{***}p < 0.001$, $^{****}p < 0.0001$, by unpaired Student *t* tests. ns = Not significant.

long-term repopulating capacity. The resulting enhanced genome stability, cell survival, and function indicate that eltrombopag may offer a new therapeutic modality for the prevention of HSPC injury induced by IR in cancer therapy, and could have implications for the treatment of genome instability syndromes such as Fanconi anemia [25]. Given the concerns raised that eltrombopag might promote clonal evolution, close monitoring is warranted in prospective clinical trials.

Acknowledgments

We thank David Stroncek, MD, and the National Institutes of Health's (NIH) Department of Transfusion Medicine (DTM) and Cell Processing Section (CPS) staff for apheresis, selection, and cryopreservation of human CD34 + cells; Kinneret Broder, RN, Therese Intrater, RN, Debbie Draper, RN, Tatyana Worthy, RN, and the outpatient clinic nursing staff for recruiting normal volunteers and providing G-CSF administration teaching to healthy subjects; Crystal Thomas, DVM, James Hawkins, DVM, and the mouse core facility staff for excellent animal care; Keyvan Keyvanfar for technical support with flow cytometry; J. Philip McCoy, PhD, Venina Dominical, PhD, and the National Heart, Lung and Blood Institute (NHLBI) flow cytometry core staff for their contribution to multispectral imaging flow cytometry; Xin Chen, PhD, for assistance with biostatistical analyses; Vera Gorbunova, PhD (University of Rochester, Rochester, NY), for providing NHEJ and HR GFP reporter plasmids; Neal S. Young, MD, Cynthia E. Dunbar, MD, and Juan Pablo Ruiz, PhD, for helpful discussions and review of the manuscript.

This work was supported by the intramural research program of the NHLBI of the NIH and a Cooperative Research and Development Agreement (CRADA) between NHLBI and GlaxoSmithKline/Novartis.

Conflict of interest disclosure

GlaxoSmithKline and Novartis, the manufacturers of eltrombopag, provided research-grade drug and research funding to the National Heart, Lung and Blood Institute under a Cooperative Research and Development Agreement (CRADA).

References

1. Jackson SP, Bartek J. The DNA-damage response in human biology and disease. Nature. 2009;461:1071–1078.
2. Lukas J, Lukas C. Molecular biology. Shielding broken DNA for a quick fix. Science. 2013;339:652–653.
3. Mohrin M, Bourke E, Alexander D, et al. Hematopoietic stem cell quiescence promotes error-prone DNA repair and mutagenesis. Cell Stem Cell. 2010;7:174–185.
4. Nijnik A, Woodbine L, Marchetti C, et al. DNA repair is limiting for haematopoietic stem cells during ageing. Nature. 2007;447:686–690.
5. Rossi DJ, Bryder D, Seita J, Nussenzweig A, Hoeijmakers J, Weissman IL. Deficiencies in DNA damage repair limit the function of haematopoietic stem cells with age. Nature. 2007;447:725–729.
6. Betermier M, Bertrand P, Lopez BS. Is non-homologous end-joining really an inherently error-prone process? PLoS Genet. 2014;10:e1004086.
7. Lieber MR. The mechanism of human nonhomologous DNA end joining. J Biol Chem. 2008;283:1–5.
8. Mladenov E, Iliakis G. Induction and repair of DNA double strand breaks: the increasing spectrum of non-homologous end joining pathways. Mutat Res. 2011;711:61–72.
9. Corneo B, Wendland RL, Deriano L, et al. Rag mutations reveal robust alternative end joining. Nature. 2007;449:483–486.
10. Grabarz A, Barascu A, Guirouilh-Barbat J, Lopez BS. Initiation of DNA double strand break repair: signaling and single-stranded resection dictate the choice between homologous recombination, non-homologous end-joining and alternative end-joining. Am J Cancer Res. 2012;2:249–268.
11. Wang H, Ronel-Perrault A, Takeda Y, Qin W, Wang H, Iliakis G. Biochemical evidence for Ku-independent backup pathways of NHEJ. Nucleic Acids Res. 2003;31:5377–5388.
12. Wang H, Rosidi B, Perrault R, et al. DNA ligase III as a candidate component of backup pathways of nonhomologous end joining. Cancer Res. 2005;65:4020–4030.
13. Boboila C, Jankovic M, Yan CT, et al. Alternative end-joining catalyzes robust IgH locus deletions and translocations in the combined absence of ligase 4 and Ku70. Proc Natl Acad Sci USA. 2010;107:3034–3039.
14. Difilippantonio MJ, Petersen S, Chen HT, et al. Evidence for replicative repair of DNA double-strand breaks leading to oncogenic translocation and gene amplification. J Exp Med. 2002;196:469–480.
15. Difilippantonio MJ, Zhu J, Chen HT, et al. DNA repair protein Ku80 suppresses chromosomal aberrations and malignant transformation. Nature. 2000;404:510–514.
16. Ferguson DO, Sekiguchi JM, Chang S, et al. The nonhomologous end-joining pathway of DNA repair is required for genomic stability and the suppression of translocations. Proc Natl Acad Sci USA. 2000;97:6630–6633.
17. Guirouilh-Barbat J, Huck S, Bertrand P, et al. Impact of the KU80 pathway on NHEJ-induced genome rearrangements in mammalian cells. Mol Cell. 2004;14:611–623.
18. Iliakis G, Wang H, Perrault AR, et al. Mechanisms of DNA double strand break repair and chromosome aberration formation. Cytogenet Genome Res. 2004;104:14–20.
19. Burma S, Chen BP, Chen DJ. Role of non-homologous end joining (NHEJ) in maintaining genomic integrity. DNA Repair (Amst). 2006;5:1042–1048.
20. de Laval B, Pawlikowska P, Petit-Cocault L, et al. Thrombopoietin-increased DNA-PK-dependent DNA repair limits hematopoietic stem and progenitor cell mutagenesis in response to DNA damage. Cell Stem Cell. 2013;12:37–48.
21. de Laval B, Pawlikowska P, Barbieri D, et al. Thrombopoietin promotes NHEJ DNA repair in hematopoietic stem cells through specific activation of Erk and NF-kappaB pathways and their target, IEX-1. Blood. 2014;123:509–519.
22. Olnes MJ, Scheinberg P, Calvo KR, et al. Eltrombopag and improved hematopoiesis in refractory aplastic anemia. N Engl J Med. 2012;367:11–19.
23. Townsley DM, Scheinberg P, Winkler T, et al. Eltrombopag added to standard immunosuppression for aplastic anemia. N Engl J Med. 2017;376:1540–1550.
24. Mao Z, Jiang Y, Liu X, Seluanov A, Gorbunova V. DNA repair by homologous recombination, but not by nonhomologous end joining, is elevated in breast cancer cells. Neoplasia. 2009;11:683–691.
25. Bagby G. Recent advances in understanding hematopoiesis in Fanconi anemia. F1000Res. 2018;7:105.

Supplementary Methods

CD34+ human hematopoietic stem and progenitor cells (HSPCs)

Human CD34+ HSPCs were obtained from male and female healthy volunteers after informed consent in accordance with the Declaration of Helsinki, under an institutional review board-approved clinical protocol (NCT00001529). Healthy volunteers underwent mobilization with a subcutaneous injection of 10 μg/kg G-CSF (Filgrastim, Amgen) for 5 days followed by leukapheresis using a Cobe Spectra Apheresis System (Terumo BCT). The mononuclear cell (MNC) concentrates were enriched in CD34+ HSPCs using a CliniMACS Plus instrument (Miltenyi Biotec) and cryopreserved prior to culture or further purification to CD34+CD38- fractions by FACS.

Cell culture and IR

Human CD34+ or CD34+CD38- cells were cultured in StemSpan SFEM II (Stem Cell Technologies) supplemented with stem cell factor (SCF; 100 ng/mL), Flt3-ligand (Flt3L; 100 ng/mL) and thrombopoietin (TPO; 100 ng/mL; all from Peprotech) or eltrombopag (3 μg/mL; Novartis) for 24 hours at 37°C, 5% CO_2. In some experiments, the culture medium was also supplemented with 10 μM NU7441 (Tocris) for DNA-PK inhibition. After 24 hours in culture, cells were placed on ice, exposed to 2Gy IR (Gammacell 1000 Irradiator, Cs-137), and cultured for an additional 1, 5 or 24 hours at 37°C, 5% CO_2. For NHEJ and HR reporter assays, HEL 92.1.7 cells were cultured in RPMI-1640 supplemented with 10% fetal bovine serum (FBS), and penicillin/streptomycin with or without TPO or eltrombopag.

Flow cytometry

To quantify DNA DSBs, apoptosis and cell death, cells were cultured and irradiated as above then cultured for an additional 1, 5, or 24 hours. Cells were stained with Annexin V-eFluor 450 and viability dye eFluor660 (eBiosciences), fixed and permeabilized with the FIX & PERM Cell Permeabilization Kit (Thermo Fisher Scientific) according to the manufacturer's instructions, and stained with rabbit monoclonal human anti-phospho-histone H2A.X (Ser139), clone 20E3, Alexa Fluor 488 conjugate (Cell Signaling Technology). All data were collected on a Fortessa flow cytometer using FACSDiva™ software version 8.0.1 (BD Biosciences) and analyzed using FlowJo software version 7.6.4 (FlowJo LLC). For sorting, freshly thawed CD34+ cells (>99% purity) were stained with anti-CD38-APC antibody (clone HB7 or HIT2, BD Pharmingen) and the CD38- fraction was collected using a FACS Aria II (BD Biosciences).

NHEJ and HR reporter assays

For evaluation of NHEJ activity, CD34+ cells were cultured for 24 hours and irradiated as above, then immediately electroporated using the Amaxa P3 Primary Cell 4D-Nucleofector Kit (Lonza) with 1 μg tdTomato plasmid as internal control, and I-SceI-digested (New England BioLabs) 3 μg NHEJ-GFP reporter plasmid. For evaluation of HR, CD34+ cells were cultured as above but cultures were extended to 4 days to allow cell cycling before IR and electroporation of 4 μg HR-GFP reporter plasmids and 1 μg tdTomato plasmid. In control groups, eltrombopag was removed during the last 24 hours of culture. To confirm findings obtained with CD34+ cells, the c-MPL expressing erythroblast cell line HEL 92.1.7 was similarly cultured for 4 days before IR and electroporation of reporter plasmids. Both NHEJ and HR plasmids were kindly provided by Dr. Vera Gorbunova (University of Rochester, NY). GFP and tdTomato expression was quantified by flow cytometry up to 24 hours after electroporation. Efficiency of DNA repair was expressed as the ratio of GFP+tdTomato+ cells to total tdTomato+ cells.

Multispectral Imaging Flow Cytometry

The number of γH2AX foci per CD34+ cell, upon stimulation schemes identical to our flow cytometry studies, was monitored and quantified using the ImageStream system (Amnis Inc.). Briefly, 2 million human CD34+ cells were stained with a Fixable Viability dye-eFluor660 (eBiosciences) at 0.2 μL/mL in PBS for 30 min at 4°C protected from light. Cells were then washed, fixed and permeabilized with the FIX & PERM Cell Permeabilization Kit (Thermo Fisher Scientific), using methanol as the fixing reagent and with minor modifications. Namely, cells were stained with 2.5 μL/mL of H2A.X during exposure to Reagent B from the FIX & PERM kit. Cells were incubated overnight at 4°C and then thoroughly washed and stained with NucBlue™ Fixed Cell Stain ReadyProbes™ reagent (DAPI, ThermoFisher Scientific) at ~2 drops/mL of media per manufacturer's recommendations. Cells were then re-suspended at 25×10^6 cells/mL in 40 μL of PBS containing 0.5% BSA. Cells that were stained with anti-γH2AX-FITC only. Fixable Viability dye-eFluor660 only and DAPI only were used for generating the compensation matrix.

Using the Inspire data acquisition software (Amnis Inc.), images of at least 10,000 live CD34+ cells were captured on channels 1 and 9 for brightfield, channel 2 for Fluorescein isothiocyanate (FITC) representing γH2AX foci, on channel 7 for DAPI nuclear counterstain, and on channel 11 for eFluor660. Excitation of the samples was performed with 405 nm, 488 nm, 658 nm and 758 nm lasers, at power settings of

30 mW, 65 mW, 50 mW and 3 mW, respectively. All images were captured using a 60X objective and enhanced depth-field mode, at a rate of 100 cell images/second.

Data analysis was performed using the IDEAS software version 6.2(.187) (Amnis Inc.). Cell classifiers were applied to record only single and focused cells upon cell area and aspect ratio. Then, live cells were selected based on the lack of fluorescence on channel 11. To quantify γH2AX foci, a compound adaptive erode and peak mask was used taking into account the fluorescence of DAPI as a counterstain for nuclear localization and the fluorescence of FITC to detect γH2AX foci, respectively: Peak([AdaptiveErode(M07, Ch7,70)],Ch2,Bright,0.0). Then, a custom spot count feature was generated to count nuclear-restricted γH2AX foci as defined by the compound mask mentioned above, per the following feature definition: Spot Count_(Peak([AdaptiveErode(M07,Ch7,70)],Ch2, Bright,0.0)_4). Using this feature, we defined populations of cells with very few foci (<3) and very high and defined foci numbers (>10), which in turn define the dynamic range of the collected images, accounting for differences in size, shape and fluorescence intensity. Additionally, an alternate masking workflow (Peak(M02,Ch2,Bright,0.0) was used in which γH2AX foci were counted across the entire cell disregarding nuclear localization yielding identical results. In order to compare γH2AX foci numbers between different cell stimulation conditions, we used histograms of foci per cell to show the population-wide distribution of γH2AX events.

Gene expression quantitative PCR array

CD34+ cells cultured and irradiated as above were collected 5 hours after IR for gene expression analysis. Total RNA was isolated using the RNeasy Plus Kit (Qiagen) according to the manufacturer's instructions. A custom real-time quantitative PCR array (RT^2 Profiler PCR Array, Qiagen) was used to determine differentially expressed genes involved in DNA damage and repair pathways, following manufacturer's instructions using the SYBR Green ROX qPCR Mastermix. See Table S1 for complete gene list. Analysis was performed using the $\Delta\Delta C_T$ method described on the PCR Array Data Analysis Web portal: http://saweb2.sabiosciences.com/pcr/arrayanalysis.php

Karyotyping

Cultured and irradiated cells were arrested in metaphases by incubation with Karyomax Colcemid Solution 10 μg/mL (Invitrogen) for 1.5 hour before harvest. Cells were collected and treated with hypotonic solution (KCl 0.075M) for 15 min at 37°C and fixed in a methanol:acetic acid mixture (3:1 vol/vol). Air-dried preparations were stained with Giemsa solution (10% Sorensen's buffer and 2% Giemsa, J.T. Baker). Well spread metaphases were blindly examined from each group for structural aberrations (n=16/group).

Colony-forming unit (CFU) assay

CFU assays were performed by plating human HSPCs cultured and irradiated as above. For each condition, the post-culture equivalent of 3,200 freshly thawed CD34+ HSPCs (corresponding to 1,400 to 2,200 cells depending on conditions) was cultured in duplicates in 1mL MethoCult H4435 Enriched Medium (Stem Cell Technologies). Colonies of greater than 50 cells were scored after 10-14 days in culture.

NSG mouse transplantation

6- to 12-week-old female NSG mice (Jackson Laboratory, stock #05557) were sublethally irradiated (280 cGy) 24 hours before tail-vein injection of human HSPCs cultured and irradiated as above. For each condition, the post-culture equivalent of 75,000 freshly sorted CD34+CD38- HSPCs (corresponding to 4-7×10^4 CD34+CD38- cells depending on conditions) was injected in each mouse. Bone marrow was collected 12 weeks post-transplantation and stained with human CD45-PE (clone HI30, BD Pharmingen). Animals were housed and handled in accordance with the guidelines set by the Committee on Care and Use of Laboratory Animals of the Institute of Laboratory Animal Resources, National Research Council (DHHS publication No. NIH 85-23), and the protocol was approved by the Animal Care and Use Committee of the National Heart, Lung, and Blood Institute.

Statistical Analysis

Results were analyzed with GraphPad Prism Software, using unpaired Student t-tests. Results are displayed as mean ± SEM and * signifies $p<0.05$, ** $p<0.01$, *** $p<0.001$, and **** $p<0.0001$.

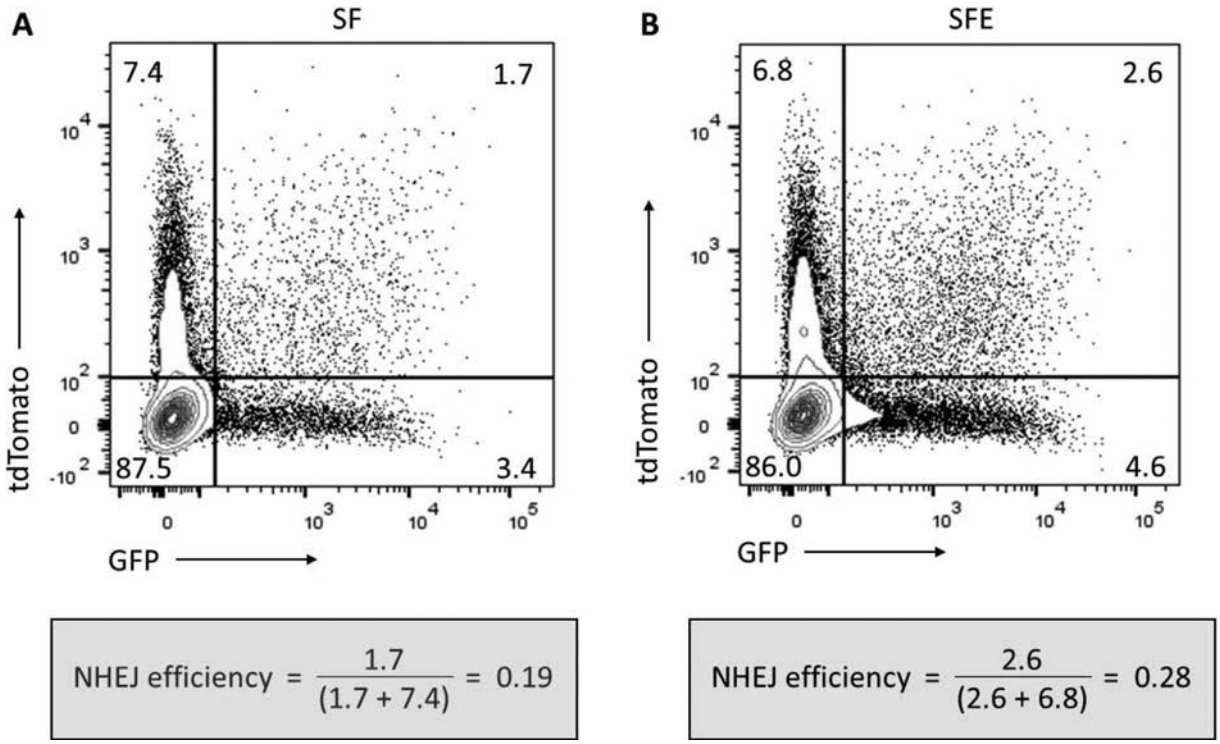

Figure E1. Efficiency of NHEJ DNA repair in human HSPCs using a reporter plasmid assay. Human CD34+ cells were cultured with (SFE) or without (SF) eltrombopag for 24 hours before IR and electroporation of NHEJ-GFP reporter plasmids and tdTomato internal control plasmids. (**A**) Representative flow cytometry plot showing GFP and tdTomato expression 24 hours after electroporation of human CD34+ cells cultured with SF (refers to Figure 1B-SF in the main manuscript). (**B**) Representative flow cytometry plot showing GFP and tdTomato expression 24 hours after electroporation of human CD34+ cells cultured with SFE (refers to Figure 1B-SFE in the main manuscript). In both panels, the bottom insets display calculations of efficiency of DNA repair mediated by the NHEJ mechanism.

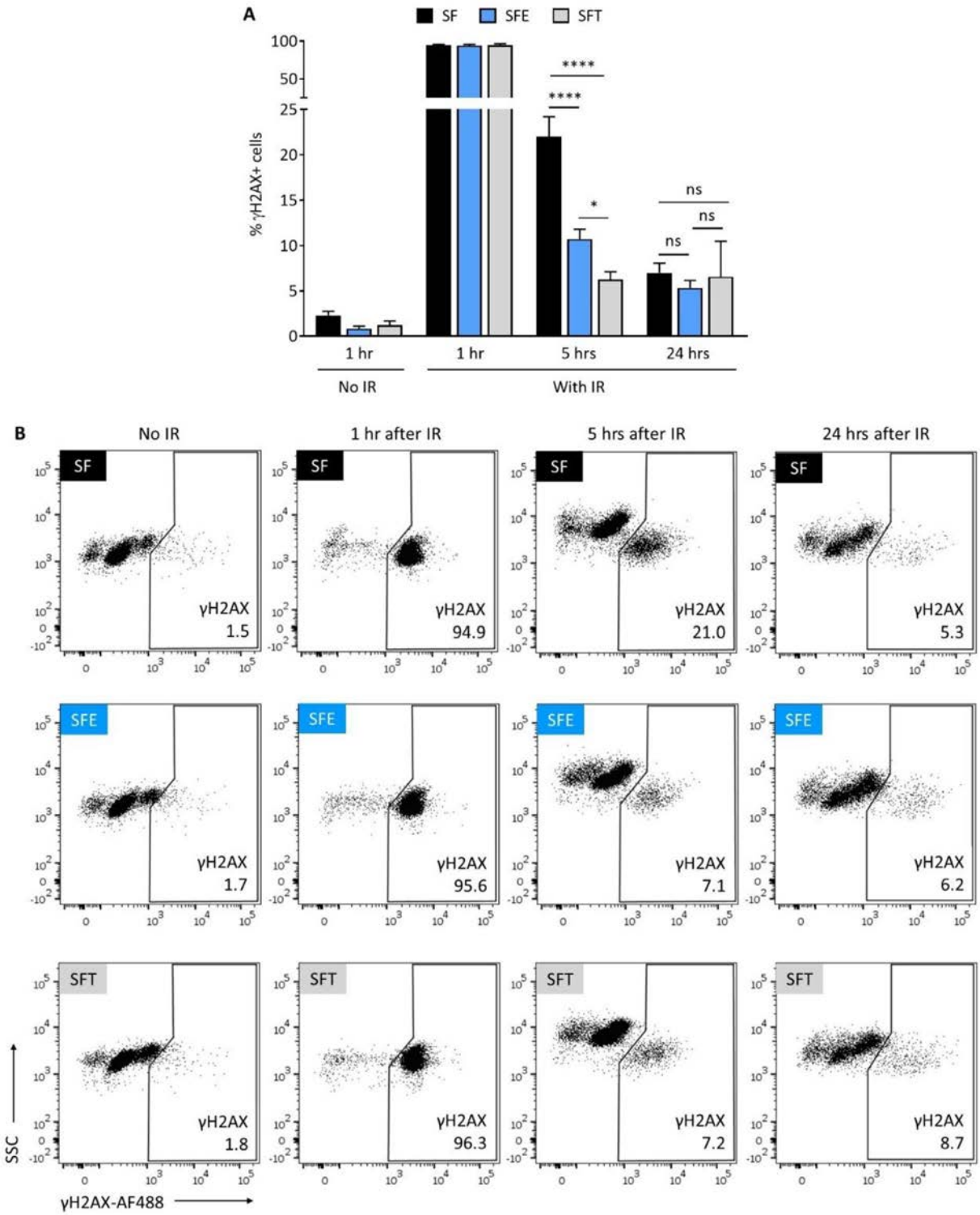

Figure E2. Eltrombopag has DNA DSB repair activity similar to TPO in human HSPCs. (**A**) Summary of H2AX phosphorylation (γH2AX) at 1, 5 and 24 hours after 2Gy IR or 1 hour after mock IR of human HSPCs cultured with SF, SFE or SFT as described in Figure 1A (n=24, from 13 independent donors). TPO's DNA repair activity was slightly superior to that of eltrombopag in human HSPCs. (**B**) Representative flow cytometry plots showing γH2AX immunostaining at 1, 5 or 24 hours post-IR or 1 hour after mock IR of human HSPCs cultured with SF (top panel), SFE (middle panel) or SFT (bottom panel). The flow cytometry gating strategy is shown in Figure E3A. In panel (A), results are displayed as mean ± SEM; * signifies $p<0.05$, **** $p<0.0001$, and ns-not significant, by unpaired Student's t-tests.

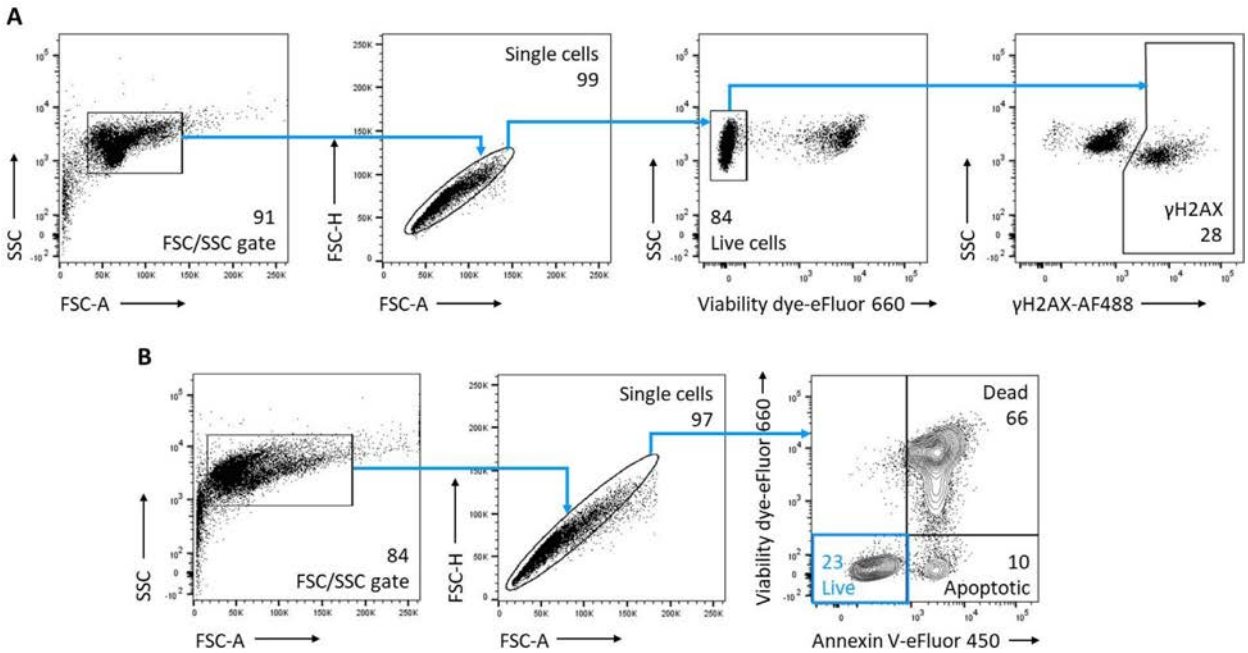

Figure E3. Flow cytometry gating strategies. (**A**) Figure exemplifying the gating strategy used for the γH2AX assay throughout this study. Representative flow cytometry plots correspond to Figure 1E (SF-5 hours) in the main manuscript. (**B**) Figure exemplifying the gating strategy used for the apoptosis/cell viability assay throughout this study. Representative flow cytometry plots correspond to Figure 2F (SF-24 hours) in the main manuscript.

Table E1. Gene list for custom RT^2 profiler PCR array

#	Gene symbol	Gene RefSeq #
1	ABL1	NM_005157
2	APEX1	NM_080649
3	APEX2	NM_014481
4	ATM	NM_000051
5	ATR	NM_001184
6	ATRIP	NM_032166
7	ATRX	NM_000489
8	ATXN3	NM_004993
9	BARD1	NM_000465
10	BAX	NM_004324
11	BBC3	NM_014417
12	BLM	NM_000057
13	BRCA1	NM_007294
14	BRCA2	NM_000059
15	BRIP1	NM_032043
16	CCNH	NM_001239
17	CCNO	NM_021147
18	CDC25A	NM_001789
19	CDC25C	NM_001790
20	CDK7	NM_001799
21	CDKN1A	NM_000389
22	CHEK1	NM_001274
23	CHEK2	NM_007194
24	CIB1	NM_006384
25	CRY1	NM_004075
26	CSNK2A2	NM_001896
27	DDB1	NM_001923
28	DDB2	NM_000107
29	DDIT3	NM_004083
30	DMC1	NM_007068
31	ERCC1	NM_001983
32	ERCC2	NM_000400
33	ERCC3	NM_000122
34	ERCC4	NM_005236
35	ERCC5	NM_000123
36	ERCC6	NM_000124
37	ERCC8	NM_000082
38	EXO1	NM_130398
39	FANCA	NM_000135
40	FANCD2	NM_033084
41	FANCG	NM_004629
42	FEN1	NM_004111
43	GADD45A	NM_001924
44	GADD45G	NM_006705
45	H2AFX	NM_002105
46	HUS1	NM_004507
47	LIG1	NM_000234
48	LIG3	NM_002311
49	LIG4	NM_002312
50	MAPK12	NM_002969
51	MBD4	NM_003925
52	MCPH1	NM_024596
53	MDC1	NM_014641
54	MGMT	NM_002412
55	MLH3	NM_014381
56	MMS19	NM_022362

(*continued*)

Table E1 (*Continued*)

(*continued*)

Table E1 (*Continued*)

#	Gene symbol	Gene RefSeq #
57	MPG	NM_002434
58	MRE11A	NM_005590
59	MSH2	NM_000251
60	MSH3	NM_002439
61	MUTYH	NM_012222
62	NBN	NM_002485
63	NEIL1	NM_024608
64	NEIL2	NM_145043
65	NEIL3	NM_018248
66	NTHL1	NM_002528
67	OGG1	NM_002542
68	PARP1	NM_001618
69	PARP2	NM_005484
70	PARP3	NM_005485
71	PCNA	NM_182649
72	PMS1	NM_000534
73	PNKP	NM_007254
74	POLB	NM_002690
75	POLD3	NM_006591
76	POLL	NM_013274
77	PPM1D	NM_003620
78	PPP1R15A	NM_014330
79	PRKDC	NM_006904
80	RAD1	NM_002853
81	RAD17	NM_002873
82	RAD18	NM_020165
83	RAD21	NM_006265
84	RAD23A	NM_005053
85	RAD23B	NM_002874
86	RAD50	NM_005732
87	RAD51	NM_002875
88	RAD51B	NM_133509
89	RAD51C	NM_058216
90	RAD51D	NM_002878
91	RAD52	NM_134424
92	RAD54L	NM_003579
93	RAD9A	NM_004584
94	RBBP8	NM_002894
95	REV1	NM_016316
96	RFC1	NM_002913
97	RNF168	NM_152617
98	RNF8	NM_183078
99	RPA1	NM_002945
100	RPA3	NM_002947
101	SIRT1	NM_012238
102	SLK	NM_014720
103	SMC1A	NM_006306
104	SMUG1	NM_014311
105	SUMO1	NM_003352
106	TDG	NM_003211
107	TOP3A	NM_004618
108	TOP3B	NM_003935
109	TOPBP1	NM_007027
110	TP53	NM_000546
111	TP53BP1	NM_005657
112	TP73	NM_005427
113	UNG	NM_003362
114	XAB2	NM_020196
115	XPA	NM_000380
116	XPC	NM_004628
117	XRCC1	NM_006297
118	XRCC2	NM_005431
119	XRCC3	NM_005432
120	XRCC4	NM_003401
121	XRCC5	NM_021141
122	XRCC6	NM_001469
123	XRCC6BP1	NM_033276
124	GAPDH	NM_002046
125	ACTB	NM_001101
126	HGDC	SA_00105
127	RTC	SA_00104
128	PPC	SA_00103

(*continued*)